Published in final edited form as:
Eur J Neurosci. 2009 February ; 29(4): 748–760. doi:10.1111/j.1460-9568.2008.06606.x.

Circuit projection from suprachiasmatic nucleus to ventral tegmental area: a novel circadian output pathway

Alice H. Luo[*] and **Gary Aston-Jones**[†]
Psychiatry Department, University of Pennsylvania, Philadelphia, PA, USA

Abstract

The suprachiasmatic nucleus (SCN) is a circadian pacemaker that synchronizes a number of vital processes. Although a great deal of research has focused on input pathways to SCN and on the central clock itself, relatively little is known about SCN output signaling pathways. The ventral tegmental area (VTA) has been extensively studied for its influence in motivated learning and, recently, for a potential role in arousal and sleep–wake regulation. Here we present data that SCN indirectly projects to VTA via the medial preoptic nucleus (MPON). Microinjection of the retrograde, transynaptic tracer pseudorabies virus (PRV) in rat VTA consistently labeled SCN neurons at time points indicative of an indirect circuit projection. To specify intermediate relay nuclei between SCN and VTA, putative relays were lesioned 1 week prior to PRV injections in VTA. Unilateral lesions of MPON reduced PRV labeling in SCN by 81.6% in the ipsilateral hemisphere and 75.8% in the contralateral hemisphere. Bilateral lesions of the caudal–dorsal lateral septum, another putative relay nucleus and dorsal injection control, did not significantly reduce PRV labeling in the SCN. Single-unit extracellular recordings under halothane anesthesia revealed a novel population of VTA neurons that selectively fired during the active circadian phase. These results show that SCN provides an indirect circuit pathway to VTA via MPON, and that VTA neurons exhibit a circadian rhythm in their impulse activity. This pathway may function in the circadian regulation of numerous behavioral processes including arousal and motivation.

Keywords

arousal; circadian; electrophysiology; pseudorabies virus; rat

Introduction

Circadian rhythms allow the organism to anticipate changes in the environment and to adjust its state accordingly. A circadian timing system consists of three main components: (i) an input pathway, (ii) a central pacemaker and (iii) an output pathway by which downstream processes can be synchronized to the pacemaker. In mammals, it is well established that the suprachiasmatic nucleus (SCN) is a central circadian pacemaker (Moore & Eichler, 1972; Stephan & Zucker, 1972; Ibuka *et al.*, 1977). However, we know very little about how SCN communicates to other systems to impart a circadian rhythmicity in behavioral and physiological processes. The SCN projects directly to a limited number of areas, primarily to other hypothalamic nuclei (Swanson & Cowan, 1975; Watts & Swanson, 1987; Watts *et al.*, 1987). The limited set of SCN projections suggest that many of these intrahypothalamic

Correspondence: Dr G. Aston-Jones, present address below. astong@musc.edu.
[*] *Present address:* Behavioral Neuroscience Research Branch, Intramural Research Program, National Institute on Drug Abuse, National Institutes of Health, Baltimore, MD 21224, USA
[†] *Present address:* Department Neurosciences, Medical University of South Carolina, Charleston, SC 29425, USA

connections may relay SCN information to various effector sites for circadian regulation of many functions, as recently demonstrated for the sleep–wake cycle (Aston-Jones *et al.*, 2001; Deurveilher & Semba, 2005; Gonzalez & Aston-Jones, 2006). The ventral tegmental area (VTA) has been implicated in reward and motivation (for review: Wise, 2004; Schultz, 2006). Interestingly, drug reward is influenced by circadian clock genes (Andretic *et al.*, 1999; Abarca *et al.*, 2002): e.g., the *Clock* mutant shows elevated cocaine preference along with increased excitability of VTA dopamine neurons (McClung *et al.*, 2005). VTA has also been implicated in sleep–wake regulation. Early studies showed that lesions of VTA decrease arousal (Jones *et al.*, 1973), and more recent work showed that VTA impulse activity fluctuates diurnally (Luo *et al.*, 2008) and varies with arousal (Lee *et al.*, 2001; Maloney *et al.*, 2002).

Here, we injected the retrograde transynaptic tracer pseudorabies virus (PRV; Bartha strain), into VTA. PRV-Bartha virions are taken up and selectively transported retrogradely from the site of injection and invade afferent somata. PRV then transynaptically infects synaptic terminals of secondary afferent neurons and is transported to parent somata where it replicates. The cycle of transport and replication repeats in a time-dependent manner and is confined to synaptically linked neurons (Card *et al.*, 1993; Jansen *et al.*, 1993; Rinaman *et al.*, 1993). These attributes have made PRV-Bartha an effective tool for the identification of extended afferent circuitry (O'Donnell *et al.*, 1997; Aston-Jones *et al.*, 2001).

Our PRV tracing showed that SCN is an indirect afferent to VTA. Cell-specific neurotoxic lesions of the medial preoptic nucleus (MPON) markedly reduced PRV labeling in SCN following VTA injections, indicating that MPON is a prominent relay in this circuit. Single-unit recordings performed during animals' active or resting circadian phases revealed that a subpopulation of VTA neurons exhibits a circadian rhythm in impulse activity. Taken together, these results indicate a novel SCN output circuit and VTA circadian rhythm that may be involved in the circadian regulation of sleep–wake and motivated behaviors.

Materials and methods

Anatomical methods

Animal surgery and microinjections—Thirty-six adult male Sprague–Dawley rats (250–415 g; Charles River Laboratories, Wilmington, MA, USA) were used. All housing and surgical procedures conformed to the BioSafety level II regulations for studies involving the use of infectious pathogens [United States Department of Health and Human Services Publication No. (Centers for Disease Control and Prevention) 88–8395; *Biosafety in Microbiological and Biomedical Laboratories*)] and were approved by the University of Pennsylvania Institutional Animal Care and Use Committee. Animals were anesthetized with ketamine–xylazine (55 mg/kg ketamine and 10 mg/kg xylazine, i.p.) and placed in a stereotaxic apparatus. For tracer injections, a mixture of PRV (Bartha strain; 1.7×10^9 pfu/mL of culture media, a gift from J. P. Card, University of Pittsburgh) and cholera toxin subunit B (CTb; 0.05% in dH_20; Sigma, St Louis, MO, USA) was unilaterally injected into the VTA through glass micropipettes (30–35 μm diameter tip). Stereotaxic coordinates for VTA injections were −5.3 mm from bregma, 8.3 mm from the cortical surface and 1.8 mm from the midline, with the injection micropipette angled medially at 10° from vertical. A volume of 480 nL of PRV/CTb was empirically found to give adequate transport while maintaining focal injection size. This volume of tracer solution was delivered over a 15-min period by brief pneumatic pulses from a controlled pressure source (Picospritzer; Parker Hannifin, Cleveland, OH, USA). The pipette was left in place for an additional 5 min to reduce upward leakage along the injection tract. For lesion studies, ibotenic acid (1% solution in artificial cerebral spinal fluid; Acros Organics, Morris Plains, NJ, USA) was injected either unilaterally (for MPON lesions; 360 nL) or bilaterally [for caudal–dorsal

lateral septum (cd-LS) lesions; 300 nL each hemisphere] into target nuclei as described for tracer injections. Stereotaxic coordinates for MPON injections were −0.7 mm from bregma, mm from the skull surface and 1.0 mm from the midline with injecting micropipette angled medially 5° from vertical. For cd-LS injection sites, the following coordinates were used: −0.27 mm from bregma, 4.0 mm from the skull surface and 1.0 mm from the midline, with the injecting micropipette angled medially at 5° from vertical.

Perfusion and tissue processing—For time-course analyses of PRV infection, animals were killed at 24, 36, 48, 52, 60 or 72 h after tracer injections (n = 2, 4, 5, 3, 5 and 2 animals at each respective time-point). Animals were deeply anesthetized with ketamine–xylazine and transcardially perfused with saline (0.9% NaCl in dH_20) followed by ~500 mL of 4% paraformaldehyde in 0.1 m sodium phosphate buffer (pH 7.4; Sigma-Aldrich, St Louis, MO, USA). Brains were removed and post-fixed overnight with the same fixative. Brains were then transferred to a solution of 20% sucrose in 0.1 m phosphate-buffered saline (PBS). Brains were cut into coronal sections (40 μm) on a cryostat and collected such that each well consisted of the entire brain at 240-μm intervals. For PRV immunohistochemistry, sections were incubated in a polyclonal rabbit anti-PRV antibody (1:5000, DP 134; gift from R. Miselis) with 2% normal donkey serum (Vector laboratories, Burlingame, CA, USA) and PBS with 0.03% Triton (Sigma-Aldrich) solution overnight at room temperature or for 2 days at 4 °C. Sections were then incubated in biotinylated donkey antirabbit antibody (1:1000; Jackson Laboratories, West Grove, PA, USA) with 2% normal donkey serum in PBS–triton solution for 2 h at room temperature followed by ABC Elite reagent (1:1000; Vector Laboratories) in PBS solution for 90 min at room temperature. Between successive incubations, sections were washed 3 × 10 min in PBS-triton. Visualization of the signal was accomplished by incubation in a 3,3-diaminobenzidine–ammonium nickel sulfate solution (Sigma-Aldrich) for 3–5 min. Immunohistochemical protocols for all other antigens were performed similarly to the above method with the following differences: (i) CTb: polyclonal goat anti-CTb (1:10,000; List Biological, Campbell, CA, USA), donkey antigoat IgG (1:1000; Jackson Laboratories) and diaminobenzidine solution; (ii) neuronal nuclei (NeuN): monoclonal mouse anti-NeuN (1:1000; Chemicon, Temecula, CA, USA), donkey antimouse IgG (1:500; Jackson Laboratories) and diaminobenzidine-nickel solution; (iii) tyrosine hydroxylase (TH): monoclonal mouse anti-TH (1:6000; DiaSorin, Stillwater, MN, USA), donkey antimouse IgG (1:500; Jackson Laboratories) and blue substrate SG (Vector Laboratories). Tissue from all injection cases was processed for PRV immunoreactivity at representative intervals (i.e., 240-μm intervals) of the entire brain. In addition, a subset of sections (e.g. from 24- and 36-h survival time-point animals) were processed for both PRV and CTb immunoreactivity at representative intervals of the entire brain. In these cases, the PRV immunoreaction was performed first, followed by the CTb immunoreaction on the same tissue. In most cases, sections corresponding to the rostral–caudal level of the VTA were also processed for both CTb and TH immunoreactivity to define the PRV/CTb injection site. In these cases, the CTb immunoreaction was performed first, followed by the TH immunoreaction on the same tissue. All sections were mounted on Superfrost Plus slides (Fisher, Fairlawn, NJ, USA) and counterstained with methyl green (Vector Laboratories). In control studies, all procedures were performed as described above, except with the respective primary antibody omitted; in all cases, this eliminated staining. Sections were examined with a Leica DM-RXA microscope. Photomicrographs were acquired with a CCD camera (Princeton Instruments Inc., Trenton NJ, USA) and processed using Openlab imaging software (Improvision Ltd., Coventry, UK). Minor adjustments in brightness and contrast were performed using Adobe Photoshop CSv.8.0 (San Jose, CA, USA).

Quantification of PRV+ neurons—Openlab image processing software was used to quantify PRV-positive (+) neurons from color digital images. Regions of interest were first

selected by using a freehand selection tool according to previously established anatomical boundaries (Swanson, 2003). The number of PRV+ neurons in regions of interest were counted with a point-counter tool. This tool simultaneously marked and counted each cell so that no cells could be counted twice and the total number of cells counted was available. Sections (240 μm apart) were taken from each animal, covering the rostral–caudal extent of each region. This corresponded to 2–4 counted sections per region, per animal. Two blinded observers determined the number of PRV+ numbers. Because there was > 90% agreement between the two observers, the counts of one of the observers was used for subsequent statistical and graphical analysis.

Electrophysiological methods

Housing—Twenty-six adult male Sprague–Dawley rats (350–425 g; Charles River Laboratories, Wilmington, MA, USA) were used for recording experiments. These rats were housed two per cage in light-tight environmental chambers under controlled conditions (21–23°C). Animals were first entrained to a 12/12-h (03.00 or 15.00 h lights on) light/dark cycle for 14 days. The 03.00 or 15.00 h lights-on regimen was chosen to account for phase advancement during the subsequent dark/dark housing (~15 min per day) so that later recording sessions occurred during normal working hours. Animals were then housed under continuously dark (dark/dark) conditions for 21–26 days before recordings began. For determination of active and rest phases during days 15–21 of dark/dark housing, animals were singly housed with photobeam detectors (San Diego Instruments, San Diego, CA, USA) in the perimeters of their cages to continuously log locomotor activity in 15-min bins. A Lomb-Scargle periodogram program (http://www.circadian.org) was used to calculate periodicity of locomotor activity. We found that locomotor activity advanced 1.5–2.0 h during the dark/dark housing week, confirming free-running circadian rhythms. The onset of the rest phase was defined as circadian time (CT) 0.

Animal surgery for electrophysiological recordings—Animals were transferred from their housing cages in light-tight transfer cages to the recording area that was dimly illuminated (< 10 lux) by a red light source. Animals were initially anesthetized with 5% halothane (Halocarbon, Riveredge, NJ, USA) in medical-grade air administered through a facemask. Black electrical tape was placed over the animals' eyes to insure they were not exposed to photic input once room lights were reilluminated to normal working lighting conditions. A tracheotomy was performed, and 2% halothane was delivered through a tracheal cannula via spontaneous respiration. Animals were placed in a stereotaxic frame, and body temperature was maintained at 36–37 °C using a thermistor-controlled electric heating pad. During recording experiments halothane concentration was kept at 1.25%. Recording sessions typically lasted ~6 h and always took place within the temporal confines of each respective circadian phase (i.e., 6 h within CT 2–10 or CT 14–22).

VTA recordings—A glass micropipette (6–10 MΩ) filled with 2% pontamine sky blue (BDH Chemicals Ltd., Poole, UK) in 0.5 m sodium acetate was used. Signals were amplified and filtered (0.5–5 kHz bandpass) using an Axoclamp 2B amplifier (Molecular Devices, Sunnyvale, CA, USA) in bridge mode and a CWE amplifier (Ardmore, PA, USA). Data were acquired and stored on a computer via an electronic interface (CED 1401, Spike2; Cambridge Electronic Design, Cambridge, UK). VTA neurons were recorded for 3–5 min to establish a mean baseline firing rate. At least 100 μm of electrode travel was required between two isolated cells to ensure recordings were from separate single units. Stereotaxic coordinates for the first VTA microelectrode penetration of a recording session were the same as those described earlier for PRV/CTb tracer injections. Multiple recording penetrations were made in each animal using a sampling grid that extended 0.4–1.2 mm from the midline, 7.0–9.0 mm from the brain surface and 4.8–6.2 mm caudal to bregma.

The VTA is well known to contain dopamine (DA) and γ-aminobutyric acid (GABA) neurons (Dahlstrom & Fuxe, 1964; Hökfelt *et al.*, 1984; Mugnaini & Oertel, 1985; Van Bockstaele & Pickel, 1995; Carr & Sesack, 2000) but more recent evidence suggests that other cell types also exist, including glutamatergic neurons (Yamaguchi *et al.*, 2007). We previously characterized a novel population of VTA neurons whose firing patterns were dependent on the diurnal cycle (Luo *et al.*, 2008). Specifically, a subset of these neurons, termed 'novel wide-spike' neurons, fired selectively during the dark phase in rats housed under light/dark housing conditions. These novel wide-spike neurons had unique electrophysiological, neurochemical and pharmacological characteristics (Luo *et al.*, 2008). As in that previous study, here a neuron was categorized as a 'novel wide-spike' neuron when the following electrophysiological characteristics were observed: (i) filtered spike duration ≤ 2.0 ms as measured by its full waveform; and (ii) fast spontaneous firing rate > 10.0 spike/s; and (iii) topographically located either ventral to at least one recorded putative GABA neuron (Steffensen *et al.*, 1998; Luo *et al.*, 2008) or among putative DA neurons (Yim & Mogenson, 1980; Grace & Bunney, 1983; Chiodo, 1988; Luo *et al.*, 2008).

Bursting analyses—For midbrain DA neurons, burst onset is typically defined as at least two spikes with an interspike interval (ISI) < 80 ms (Grace & Bunney, 1983, 1984). However, this criterion is not satisfactory for rapidly firing cells such as our 'novel wide-spike' cells, e.g., those whose mean ISIs are close to or < 80 ms. An alternative method was employed in which the cell's bursting activity was not directly proportional to firing rate. This discharge density histogram (see Luo *et al.*, 2008 for detailed methodology) method was employed to characterize the bursting activity of both putative DA neurons and novel wide-spike neurons.

Statistical analyses—Results are expressed as the mean ± SEM, unless otherwise noted. For lesioned animals, cell counts were statistically compared to matched (i.e. same survival time-point) intact animals used in the initial PRV time-course study. The following parametric tests were used, as appropriate: unpaired Student's *t*-test and one-way ANOVA followed by Newman–Keul's post-test. For nonparametric data sets, the Fisher Exact test and Mann–Whitney *U* were employed where appropriate.

Results

PRV injection in VTA resulted in time-dependent retrograde transport to SCN

PRV labeling was found in SCN neurons beginning at 48 h survival in all cases with accurate injections in VTA. SCN labeling was not present in cases in which injection sites were localized to structures nearby, but outside of, VTA (e.g. red nucleus, substantia nigra pars compacta or reticulata; data not shown). Figure 1A–C shows the time course for PRV labeling in SCN at 36, 48 and 60 h after VTA injection. At 36 h, PRV labeling was absent in the SCN although known primary afferents to VTA, such as nucleus accumbens, lateral hypothalamus and pedunculopontine nucleus, contained PRV labeling.

Because PRV is avidly transported away from the injection site, the conventional retrograde tracer CTb was included in the injection solution to localize injection sites and to differentiate between direct and indirect afferents, as in other studies (Card *et al.*, 1999; Chen *et al.*, 1999; Aston-Jones & Card, 2000; Aston-Jones *et al.*, 2001). Figure 2A schematically shows the boundaries of CTb immunoreactivity at the injection sites for animals sacrified 48 h after injection. All of these injections resulted in PRV retrograde labeling in SCN. Figure 2B shows CTb immunoreactivity at the largest extent of the injection site for one of these cases (48P10). TH staining of adjacent sections (Fig. 2C) revealed that these injections were largely localized within the VTA. Figure 3 shows

retrograde labeling in nucleus accumbens (NAC) with CTb and PRV at 36 h following injection. PRV labeling in this and other direct VTA afferents was consistently present at 36 h, and continued to increase at longer survival time-points. However, PRV was not observed in SCN until 48 h after injection in VTA (Fig. 1B), indicating that SCN may be an indirect afferent to VTA. In addition, CTb did not appear within SCN at any time point. PRV labeling in SCN first appeared (at 48 h post-injection) in the ventrolateral aspect of the ipsilateral SCN. By 60 h, labeling was dense throughout both the ipsilateral and contralateral SCN nuclei, although labeling remained stronger ipsilateral to the injection in VTA (Fig. 1C).

MPON is a relay in the SCN-VTA circuit

Evidence here and elsewhere (Phillipson, 1979; Geisler & Zahm, 2005) indicates that SCN does not directly innervate VTA, and we surmised that the SCN labeling above was due to an indirect circuit projection from SCN to VTA. We therefore investigated possible intermediate nuclei that might serve as a relay in an SCN circuit projection to VTA. Nuclei that met the following criteria were considered candidate relays: (i) known direct targets of SCN projections; (ii) known direct afferents to VTA; and (iii) consistent PRV labeling at ≤ 36 h following injection, i.e., time points prior to PRV labeling in the SCN. Nuclei that satisfied these criteria included the medial preoptic area, the lateral septum, the bed nucleus of the stria terminalis, the paraventricular nucleus of the hypothalamus, and the lateral hypothalamus. The number of PRV+ neurons at 36 h post-injection was low for the bed nucleus of the stria terminalis (4.0 ± 1.3 labeled neurons per section in the ipsilateral hemisphere; $n = 4$ animals), paraventricular nucleus of the hypothalamus (3.4 ± 1.2 neurons) and the lateral hypothalamus (5.1 ± 1.1 neurons). In contrast, Fig. 4 shows that, at 36 h survival, CTb+ and PRV+ neurons were much more numerous within specific subregions of the medial preoptic area and lateral septum, corresponding to the MPON (Simerly *et al.*, 1986; Simerly & Swanson, 1988) and the cd-LS (Risold & Swanson, 1997a,b), respectively. These two areas contained the most labeled neurons at this time point of any structures analyzed. PRV+ labeling was higher at 36 h survival in MPON and the cd-LS than in nearby nuclei, including known SCN efferents (paraventricular nucleus of the thalamus, paraventricular nucleus of the hypothalamus and ventromedial hypothalamus; one-way ANOVA, Neuman–Keuls post-test, $F_{(7,104)} = 5.53$, $p < 0.05$; $n = 4$ animals, all regions counted from same animals). Figure 5 shows that labeling in the MPON and cd-LS increased with longer survival times (48 or 60 h). Because of the consistency and density of labeling in the MPON and cd-LS, these subregions were the focus of subsequent lesions to identify relay nuclei.

Lesion of MPON, but not of cd-LS, reduced PRV labeling in SCN

To test whether MPON and/or cd-LS are intermediate nuclei in an SCN-VTA pathway, separate experiments were performed in which we lesioned MPON or cd-LS with ibotenic acid prior to PRV/CTb injections into VTA. Five to seven days after an ibotenic acid lesion, PRV/CTb was microinjected in VTA and rats were scarified either 48 or 52 h later. We picked these time points because of the abundance of PRV labeling in the SCN of intact rats without significant PRV-induced cellular necrosis.

Because MPON contains temperature-regulatory neurons, bilateral lesions of MPON frequently results in hyperthermia-induced death (Satinoff *et al.*, 1976). Therefore, lesions in MPON were made unilaterally, ipsilateral to the VTA injection, consistent with the observation that most PRV and CTb labeling in MPON was ipsilateral to VTA injections. Figure 6B shows PRV labeling in SCN at 48 h post-injection from animals with excitotoxic lesions of MPON. These MPON lesions resulted in an 81.6% reduction in the number of ipsilateral SCN neurons that were labeled with PRV (intact, 177.1 ± 19.9 labeled cells per

section, $n = 5$ animals; lesioned, 32.6 ± 16.5 labeled cells per section, $n = 4$ animals; t-test, $t_{15} = 4.38$, $P < 0.001$; Fig. 6 PRV labeling in the contralateral SCN was also reduced in these animals, by 75.8% (intact, 40.4 ± 24.8 labeled cells per section; lesioned, 9.8 ± 4.8 labeled cells per section; $t_{15} = 3.02$, $P < 0.01$). MPON-lesioned animals killed at 52 h also had significantly reduced PRV labeling, exhibiting a 61.5% reduction in ipsilateral SCN (intact, 194.5 ± 27.0 labeled cells per section, $n = 3$ animals; lesioned, 74.9 ± 3.6 labeled cells per section, $n = 3$ animals; t-test, $t_{13} = 4.08$, $P = 0.001$) and a 69.2% reduction in contralateral SCN (intact, 71.4 ± 6.9 labeled cells per section; lesioned, 22.0 ± 6.4 labeled cells per section; $t_{13} = 3.72$, $P < 0.01$).

Figure 7 shows schematic outlines in our four MPON lesion cases (with subsequent 48 h PRV post-injection times) of their ibotenic acid lesion (Fig. 7A) and PRV injection sites (Fig. 7B). Based on our earlier time-course studies in intact rats, we found that PRV labeling was evident in surrounding subnuclei of the MPON at 48 h post-injection, and therefore PRV immunoreactivity was a good marker for defining the perimeter of the lesioned area. Figure 7C, left, contains representative photomicrographs of PRV labeling from intact and MPON-lesioned animals. These results confirmed that the extent of the lesioned area was largely restricted to the MPON subregion of the preoptic area.

The decrease in PRV labeling in SCN following MPON lesions appears to be due to direct manipulation of the SCN–MPON–VTA pathway. Figure 7C, right, shows that labeling in other areas that project to VTA, such as NAC, did not significantly change in MPON-lesioned animals (23.3% reduction: ipsilateral intact, 163.2 ± 34.5 labeled cells per section, $n = 5$ animals; ipsilateral lesioned, 125.2 ± 42.4 labeled cells per section, $n = 4$ animals; t-test, $t_9 = 0.70$, $P = 0.50$), indicating that lesions of the MPON did not result in nonspecific changes in other aspects of VTA afferent circuitry.

In contrast to MPON-lesioned animals, cd-LS-lesioned animals did not show significantly reduced PRV labeling in the SCN. Animals with cd-LS lesions were sacrified at 48 h after PRV injections into VTA because this time-point revealed strongly decreased PRV labeling in SCN of MPON-lesioned animals. Figure 6C and E show that bilateral lesions of cd-LS resulted in a slight, but nonsignificant, reduction in the number of PRV-labeled neurons in SCN ipsilateral to the VTA injected 48 h earlier (15.0% reduction: intact, 177.1 ± 19.9 labeled cells per section, $n = 5$ animals; lesioned, 150.6 ± 31.1 labeled cells per section, $n = 8$ animals; t-test, $t_{28} = 0.88$, $P = 0.39$). Interestingly, cd-LS lesioned animals exhibited increased PRV labeling in contralateral SCN (57.9% increase: intact, 40.4 ± 24.8 labeled cells per section; lesioned, 96.0 ± 27.7 labeled cells per section, $t_{28} = 2.38$, $P < 0.05$). This may be due to increased virion availability in the SCN-VTA circuit in lesioned animals, and will be discussed below. Regardless, lesion of the cd-LS did not result in reduced SCN labeling. It is also notable that the cd-LS lesion sites were along a similar stereotaxic tract as used for the MPON lesions. Therefore, the absence of effect of cd-LS lesions on SCN labeling from VTA indicates that the loss of labeling following MPON lesions was not due to leakage of ibotenate from the MPON dorsally along the injection tract.

Figure 8 shows schematic outlines from these cd-LS lesion cases of their respective ibotenic acid lesion (Fig. 8B) and PRV injection sites (Fig. 8A). Based on our previous time-course studies in intact animals, even by 48 h PRV labeling in the lateral septum was still largely restricted to the cd-LS subregion, such that PRV immunoreactivity itself was not sufficient to define the perimeter of the lesioned area (Fig. 8C, left). Therefore, the neuronal marker NeuN was used to define the extent of these lesions (Fig. 8C, right). NeuN immunoreactivity showed that ibotenic acid effectively lesioned virtually all of the cd-LS, and that lesions were mostly confined to the caudal–dorsal aspect of lateral septum and spared other subregions (e.g., ventral E lateral septum).

VTA novel wide-spike neurons exhibited a circadian rhythm in impulse activity

We performed single-unit extracellular recordings of VTA neurons in halothane-anesthetized rats housed under continuously dark conditions. Surprisingly, putative DA neurons did not show any changes in firing rate (resting phase DA neuron firing rate, 3.9 ± 0.2 spikes/s, $n = 101$ cells, 13 animals; active phase DA neuron firing rate, 3.9 ± 0.2 spikes/s, $n = 107$ cells, 13 animals; t-test, $t_{206} = 0.15$, $P = 0.88$) or bursting activity (resting phase DA neuron spikes-in-bursts, 23.1 ± 2.4%; active phase DA neuron spikes-in-bursts, 21.6 ± 2.0%; Mann–Whitney $U = 3764$, $P = 0.66$) as a function of recording in the resting vs. active circadian phases. Putative GABA neurons also failed to show differences in firing rate as a function of circadian phase (resting phase GABA neuron firing rate, 14.5 ± 1.4 spikes/s, $n = 48$ cells, 13 animals; active phase GABA neuron firing rate, 12.7 ± 1.5 spikes/s, $n = 54$ cells, 13 animals; t-test, $t_{100} = 0.90$, $P = 0.37$). However, we did observe circadian-dependent changes in a population of novel wide-spike neurons that we previously described in VTA recordings (Luo *et al.*, 2008). Under light/dark housing conditions, these novel neurons selectively fired during the dark (active) phase (Luo *et al.*, 2008). In the current study this pattern persisted under dark/dark housing conditions, i.e., novel wide-spike neurons were preferentially found during the active circadian phase (10 of 12 novel wide-spike cells, or 83.3% of the total novel wide-spike population; $n = 8$ animals; Fig. 9B). Novel wide-spike neurons represented 6.2% of total cells recorded during the active phase (10 of 161 cells; $n = 13$ animals) and only 1.3% of total cells recorded during the resting phase (2 of 154 cells; $n = 13$ animals; $P < 0.05$, Fisher exact test). Figure 9A and C shows that the electrophysiological characteristics of these novel cells were similar to those previously reported for novel wide-spike neurons (Luo *et al.*, 2008), i.e., wide spike durations (full waveform, 2.21 ± 0.05 ms; start of waveform to peak of initial negative trough, 0.99 ± 0.05 ms), fast firing rates (19.8 ± 2.7 spikes/s), and low bursting activity (6.5 ± 3.5% of spikes in bursts; $n = 12$ cells, eight animals). These data indicate that novel wide-spike neurons exhibited a circadian rhythm in their firing activity, i.e., they preferentially fired during the active circadian phase regardless of light exposure.

The number of spontaneously active neurons found per electrode track was also calculated. This ‘cell/track’ measure has been used extensively as an indirect measure of population activity (Bunney & Grace, 1978; White & Wang, 1983; Floresco *et al.*, 2001). Of all the examined VTA neuronal subtypes (e.g., novel wide-spike, putative DA or GABA neurons), the novel wide-spike neurons were the only subtype to show increased cells/track during the active circadian phase (active phase, 0.15 ± 0.05 cell/track, $n = 13$ animals, 69 tracks; resting phase, 0.03 ± 0.02, $n = 13$ animals, 78 tracks; Mann–Whitney $U = 2408$, $P = 0.02$; Fig. 9D). These results show that novel wide-spike neuron firing rhythmicity is not dependent on light input and is consistent with the possibility that SCN activates novel neurons during the active period.

Discussion

Injection of the retrograde transynaptic tracer PRV into VTA labeled SCN neurons at delays consistent with an indirect circuit projection. Experiments combining lesions and PRV labeling revealed that MPON, but not cd-LS, is a major intermediary in this SCN-VTA projection. Electrophysiological recordings of VTA neurons revealed a possible functional consequence of this circuit; a population of novel VTA neurons was identified that exhibited a strong circadian rhythm in firing activity. Taken together, these data define a novel circuit projection from the SCN to the VTA via the MPON that we hypothesize produces a circadian rhythm in VTA neurons.

Technical considerations

Because PRV is readily transported away from the site of injection, identification of the injection site can be difficult (Card *et al.*, 1999; Chen *et al.*, 1999). Therefore, CTb was co-injected to specify injection location and help determine direct afferent neurons (Aston-Jones & Card, 2000). Because of the large size of PRV virions (~180 nm), injected CTb diffuses more than PRV, and CTb therefore provides an overestimate of the spread of injected PRV (O'Donnell *et al.*, 1997; Chen *et al.*, 1999). We found that 480 nL of 1.7×10^9 pfu/mL of PRV plus 0.05% CTb labeled known primary afferents at 36 h of survival while maintaining focal injection sites. This produced an injection size, speed and anatomical pattern of retrograde labeling similar to that seen with PRV injections in other circuits (Aston-Jones *et al.*, 2001).

As with any tracer, it is possible that PRV was taken up by fibers of passage. However, Chen *et al.* (1999) found that PRV is taken up by fibers of passage to a smaller extent than other tracers. In addition, SCN has never been reported to be a direct VTA afferent, even with tracers that are more susceptible to uptake by fibers of passage such a horseradish peroxidase (Phillipson, 1979). The possibility of uptake by damaged fibers was also tempered by our use of a controlled pneumatic pressure injection system and slow infusion rate.

We reasoned that, if a nucleus is part of the SCN-VTA circuit, elimination of the corresponding somata should interrupt a pathway for PRV virions to be transported to the SCN. This lesion strategy was successfully employed previously in our lab (Aston-Jones *et al.*, 2001) and by others (Pickard *et al.*, 2002; Smeraski *et al.*, 2004) to delineate multisynaptic circuits. Using this strategy, we found that lesion of MPON significantly reduced PRV labeling in SCN, implicating MPON as a relay in this circuit. In contrast, lesion of cd-LS did not reduce PRV labeling in SCN, ruling out cd-LS as a relay. Furthermore, cd-LS served as a control for upward leakage of ibotenate in MPON lesion cases because the cd-LS is dorsal to, and along the trajectory of, the MPON injection pipette.

Surprisingly, we found that bilateral ibotenate lesions of cd-LS increased PRV labeling in contralateral SCN. These results might reflect the fact that PRV infection is highly sensitive to terminal field density (Card *et al.*, 1999). Both MPON and cd-LS are major afferents to VTA, but only MPON seems to be a major node in the SCN-VTA circuit. Because of their overlapping terminal fields within VTA, it is possible that lesion of cd-LS terminals increased PRV virion availability for uptake by MPON terminals and subsequent transneuronal retrograde transport to SCN. It is currently not known why this increase occured in the contralateral but not the ipsilateral SCN. One possibility is that, because the contralateral MPON projection to VTA is sparser than the ipsilateral projection, it has greater potential for more efficacious viral uptake than the ipsilateral projection. It is possible that a ceiling effect exists for the ipsilateral projection where it would not be possible to see substantially larger numbers of labeled neurons; this is consistent with the large proportion of ipsilateral SCN neurons that are already PRV+ at 48 h. Additional experiments are needed to test this and other possibilities.

Elements of the SCN-to-VTA projection circuit

Our results indicate that SCN indirectly projects to VTA, and that MPON is a major intermediary. However, it is unclear how many additional nuclei or subnuclei are contained in this circuit. For example, it has been reported that rostral VTA receives inputs from caudal VTA, but not the converse (Ferreira *et al.*, 2008). It is possible that rostral VTA does not receive a major input from the MPON, but participates in the SCN-MPON circuit

through its connection with caudal VTA. Such fine resolution would require additional experiments. Moreover, MPON may not be the only intermediary in the overall SCN-VTA circuit. Nevertheless, our results indicate that MPON is a dominant intermediary nucleus given the dramatic reduction in PRV labeling in SCN after MPON lesions.

We consistently observed that PRV labeling occurred first in the ventrolateral region of SCN, with subsequent spread to the rest of SCN including the dorsomedial region. This result is consistent with previous studies of SCN circuit projections (Aston-Jones *et al.*, 2001), and with findings that dorsomedial SCN projects densely to ventrolateral SCN but not *vice versa* (Leak *et al.*, 1999). Numerous studies have shown that the SCN is a heterogeneous structure with differing characteristics within its subregions, although not necessarily always mutually exclusive in function (Moore, 1996, 1997; Yan *et al.*, 1999; Hamada *et al.*, 2001; de la Iglesia *et al.*, 2004; Morin *et al.*, 2006). Our results indicate that information conveyed to VTA probably arises from the ventrolateral region of SCN, and that other subregions of SCN may influence the VTA via projections to the ventraolateral SCN.

Circadian rhythm of VTA novel wide-spike population

A population of 'novel wide-spike' neurons that we previously characterized (Luo *et al.*, 2008) exhibited a circadian rhythm in impulse activity in the present study. These neurons were infrequently found in the resting phase; this could be either because they are silent at this time, in which case we would not have detected them, or because they are slower-firing during the resting phase (i.e. < 10.0 spikes/s), in which case they would have met the classic criteria for midbrain DA neurons (Yim & Mogenson, 1980; Grace & Bunney, 1983; Chiodo, 1988). Our results for the number of spontaneously active cells per electrode track indicate that the former possibility is more likely. We found that novel wide-spike neurons were the only VTA cells to exhibit an increase in cells/track, and no VTA cell type showed a decrease in cells/track, during the active phase. This was true for animals housed in light/dark (Luo *et al.*, 2008) or dark/dark conditions (present study). Thus, we hypothesize that novel wide-spike neurons are silent during the resting phase and only fire during the active phase.

Circadian clock genes are expressed in many areas other than SCN. *Per* is expressed in rat VTA (Abe *et al.*, 2002) and *Clock* is expressed in mouse VTA (McClung *et al.*, 2005). However, *Per* expression does not exhibit circadian oscillations (Abe *et al.*, 2002) and *Clock* expression has not been reported to oscillate. Although not definitive, these results suggest that our observed circadian rhythm is not due to intrinsic oscillations of circadian clock genes within the VTA. Regardless of whether VTA circadian rhythms are generated intrinsically and entrained by the SCN, or entirely driven by SCN, our results are consistent with the hypothesis that the SCN-MPON-VTA pathway has a functional output. Additional experiments are needed to confirm these possibilities.

Role of MPON in an SCN-VTA circuit

Anatomically, MPON is situated slightly rostral and dorsal to the SCN. While the densest pathway from the SCN is to the paraventricular nucleus and subparaventricular nucleus of the hypothalamus (Vrang *et al.*, 1995), the SCN projection to MPON is part of a moderately dense pathway that projects rostrally and dorsally (Watts & Swanson, 1987; Watts *et al.*, 1987). Axons from this pathway terminate in the medial preoptic area including the MPON, while other axons continue to course dorsally to terminate in the rostral pole of paraventricular nucleus of the thalamus (Watts & Swanson, 1987; Watts *et al.*, 1987).

The MPON is a heterogeneous and sexually dimorphic structure that has been implicated in a number of processes, including sexual behavior (for review: Hull *et al.*, 2002). Lesioning

MPON in one hemisphere and VTA in the other reduces preference for a receptive female and eliminates copulation (Brackett & Edwards, 1984; Edwards & Einhorn, 1986). It has been suggested that MPON works in conjunction with VTA to integrate motivational and appetitive aspects of sexual behavior with somatomotor responses to generate the full behavioral sexual repertoire (Everitt, 1990; Hull, 1995). Given the circadian rhythmicity of mating behavior (Harlan *et al.*, 1980; Stefanick, 1983), it is possible that the SCN-MPON-VTA circuit temporally coordinates motivational aspects of mating behavior.

The majority of MPON neurons are sleep-active (Kaitin, 1984), and lesions of MPON reduce sleep (Asala *et al.*, 1990; John & Kumar, 1998). Also, Fos expression in MPON is directly proportional to the homeostatic pressure to sleep (Pompeiano *et al.*, 1994; Cirelli *et al.*, 1995). The projection from MPON to VTA appears to be primarily inhibitory (Maeda & Mogenson, 1980). Given that a large proportion of MPON neurons are sleep-active, and sleep predominately occurs during the resting phase, it is possible that VTA novel wide-spike neurons are tonically inhibited by MPON during the resting phase. During the active phase, novel wide-spike neurons may be released from this MPON inhibition. This is consistent with our finding that cells/track increase for novel neurons in active vs. resting periods.

An SCN-MPON-VTA circuit in the circadian regulation of reward

Reward processing is also influenced by circadian factors. Terman & Terman (1970) first showed that rewarding intracranial brain stimulation exhibits a robust circadian rhythm. Since then, other animal models of reward, including drug self-administration, conditioned place preference and locomotor sensitization have shown that time of day can profoundly influence reward processing (Baird & Gauvin, 2000; Abarca *et al.*, 2002; Roberts *et al.*, 2002). Interestingly, animals with mutations of *Clock* or *Period*, core circadian genes in SCN, exhibit altered responses in drug-seeking paradigms (Abarca *et al.*, 2002; McClung *et al.*, 2005). The mechanism by which circadian clock genes modulate reward circuitry is unknown, but one possibility is that animals with compromised SCN function affect downstream reward regulatory sites such as the VTA. Our SCN-MPON-VTA circuit may be a substrate for the circadian regulation of reward.

Conclusions

Because of SCN's limited terminal field, it has been hypothesized that structures such as MPON may function as circadian relays to major arousal systems (Deurveilher & Semba, 2005). Our results showing a synaptically linked SCN-MPON-VTA circuit are consistent with that possibility. Given existing knowledge about SCN, MPON and VTA, we speculate that this circuit may be involved in circadian regulation of behavioral processes such as sleep–wake, sexual motivation and reward. Further studies are needed to test these and other possible roles of this circuit in physiological and behavior processes.

Acknowledgments

We thank Dr Yan Zhu for technical advice, and Nataliya Biskup for assistance with tissue processing. This work was supported by PHS grants R37 DA06214, R01 017289 and F31 MH071093.

Abbreviations

+	positive
cd-LS	caudal–dorsal lateral septum

CT	circadian time
CTb	cholera toxin subunit B
DA	dopamine
GABA	γ-aminobutyric acid
MPON	medial preoptic nucleus
NAC	nucleus accumbens
NeuN	neuronal nuclei
PBS	phosphate-buffered saline
PRV	pseudorabies virus
SCN	suprachiasmatic nucleus
TH	tyrosine hydroxylase
VTA	ventral tegmental area

References

Abarca C, Albrecht U, Spanagel R. Cocaine sensitization and reward are under the influence of circadian genes and rhythm. Proc Natl Acad Sci USA. 2002; 99:9026–9030. [PubMed: 12084940]

Abe M, Herzog ED, Yamazaki S, Straume M, Tei H, Sakaki Y, Menaker M, Block GD. Circadian rhythms in isolated brain regions. J Neurosci. 2002; 22:350–356. [PubMed: 11756518]

Andretic R, Chaney S, Hirsh J. Requirement of circadian genes for cocaine sensitization in Drosophila. Science. 1999; 285:1066–1068. [PubMed: 10446052]

Asala SA, Okano Y, Honda K, Inoue S. Effects of medial preoptic area lesions on sleep and wakefulness in unrestrained rats. Neurosci Lett. 1990; 114:300–304. [PubMed: 2402338]

Aston-Jones G, Card JP. Use of pseudorabies virus to delineate multisynaptic circuits in brain: opportunities and limitations. J Neurosci Methods. 2000; 103:51–61. [PubMed: 11074095]

Aston-Jones G, Chen S, Zhu Y, Oshinsky ML. A neural circuit for circadian regulation of arousal. Nat Neurosci. 2001; 4:732–738. [PubMed: 11426230]

Baird TJ, Gauvin D. Characterization of cocaine self-administration and pharmacokinetics as a function of time of day in the rat. Pharmacol Biochem Behav. 2000; 65:289–299. [PubMed: 10672982]

Brackett NL, Edwards DA. Medial preoptic connections with the midbrain tegmentum are essential for male sexual behavior. Physiol Behav. 1984; 32:79–84. [PubMed: 6718539]

Bunney BS, Grace AA. Acute and chronic haloperidol treatment: comparison of effects on nigral dopaminergic cell activity. Life Sci. 1978; 23:1715–1727. [PubMed: 31529]

Card JP, Rinaman L, Lynn RB, Lee BH, Meade RP, Miselis RR, Enquist LW. Pseudorabies virus infection of the rat central nervous system: ultrastructural characterization of viral replication, transport, and pathogenesis. J Neurosci. 1993; 13:2515–2539. [PubMed: 8388923]

Card JP, Enquist LW, Moore RY. Neuroinvasiveness of pseudorabies virus injected intracerebrally is dependent on viral concentration and terminal field density. J Comp Neurol. 1999; 407:438–452. [PubMed: 10320223]

Carr DB, Sesack SR. GABA-containing neurons in the rat ventral tegmental area project to the prefrontal cortex. Synapse. 2000; 38:114–123. [PubMed: 11018785]

Chen S, Yang M, Miselis RR, Aston-Jones G. Characterization of transsynaptic tracing with central application of pseudorabies virus. Brain Res. 1999; 838:171–183. [PubMed: 10446330]

Chiodo LA. Dopamine-containing neurons in the mammalian central nervous system: electrophysiology and pharmacology. Neurosci Biobehav Rev. 1988; 12:49–91. [PubMed: 3287242]

Cirelli C, Pompeiano M, Tononi G. Sleep deprivation and c-fos expression in the rat brain. J Sleep Res. 1995; 4:92–106. [PubMed: 10607147]

Dahlstrom A, Fuxe F. Evidence for the existence of monoamine containing neurons in the central nervous system. I Demonstration of monoamines in the cell bodies of brain stem neurons. Acta Physiol Scand. 1964; 62:1–55. [PubMed: 14210262]

Deurveilher S, Semba K. Indirect projections from the suprachiasmatic nucleus to major arousal-promoting cell groups in rat: implications for the circadian control of behavioural state. Neuroscience. 2005; 130:165–183. [PubMed: 15561433]

Edwards DA, Einhorn LC. Preoptic and midbrain control of sexual motivation. Physiol Behav. 1986; 37:329–335. [PubMed: 3488558]

Everitt BJ. Sexual motivation: a neural and behavioural analysis of the mechanisms underlying appetitive and copulatory responses of male rats. Neurosci Biobehav Rev. 1990; 14:217–232. [PubMed: 2190121]

Ferreira JG, Del-Fava F, Hasue RH, Shammah-Lagnado SJ. Organization of ventral tegmental area projections to the ventral tegmental area-nigral complex in the rat. Neuroscience. 2008; 153:196–213. [PubMed: 18358616]

Floresco SB, Todd CL, Grace AA. Glutamatergic afferents from the hippocampus to the nucleus accumbens regulate activity of ventral tegmental area dopamine neurons. J Neurosci. 2001; 21:4915–4922. [PubMed: 11425919]

Geisler S, Zahm DS. Afferents of the ventral tegmental area in the rat-anatomical substratum for integrative functions. J Comp Neurol. 2005; 490:270–294. [PubMed: 16082674]

Gonzalez MM, Aston-Jones G. Circadian regulation of arousal: role of the noradrenergic locus coeruleus system and light exposure. Sleep. 2006; 29:1327–1336. [PubMed: 17068987]

Grace AA, Bunney BS. Intracellular and extracellular electrophysiology of nigral dopaminergic neurons—1. Identification and characterization. Neuroscience. 1983; 10:301–315. [PubMed: 6633863]

Grace AA, Bunney BS. The control of firing pattern in nigral dopamine neurons: burst firing. J Neurosci. 1984; 4:2877–2890. [PubMed: 6150071]

Hamada T, LeSauter J, Venuti JM, Silver R. Expression of Period genes: rhythmic and nonrhythmic compartments of the suprachiasmatic nucleus pacemaker. J Neurosci. 2001; 21:7742–7750. [PubMed: 11567064]

Harlan RE, Shivers BD, Moss RL, Shryne JE, Gorski RA. Sexual performance as a function of time of day in male and female rats. Biol Reprod. 1980; 23:64–71. [PubMed: 7191337]

Hökfelt, T.; Martensson, R.; Björklund, A.; Kleinau, S.; Goldstein, M. Distributional Map of tyrosine-hydroxylase-immunoreactive neurons in the rat brain. In: Bjorklund, A.; Hokfelt, T., editors. Handbook of Chemical Neuroanatomy. Elsevier; Amsterdam: 1984. p. 277-379.

Hull, EM. Dopaminergic influences on male rat sexual behavior. In: Micevych, PE.; Hammer, RP., Jr, editors. Neurobiological Effects of Sex Steroid Hormones. Cambridge University Press; Cambridge, UK: 1995. p. 234-253.

Hull, EM.; Meisel, RL.; Sachs, BD. Male sexual behavior. In: Pfaff, DW.; Arnold, AP.; Etgen, AM.; Fahrbach, SE.; Rubin, RT., editors. Hormones, Brain and Behavior. Academic Press; San Diego: 2002. p. 3-137.

Ibuka N, Inouye SI, Kawamura H. Analysis of sleep-wakefulness rhythms in male rats after suprachiasmatic nucleus lesions and ocular enucleation. Brain Res. 1977; 122:33–47. [PubMed: 837222]

de la Iglesia HO, Cambras T, Schwartz WJ, Diez-Noguera A. Forced desynchronization of dual circadian oscillators within the rat suprachiasmatic nucleus. Curr Biol. 2004; 14:796–800. [PubMed: 15120072]

Jansen AS, Farwell DG, Loewy AD. Specificity of pseudorabies virus as a retrograde marker of sympathetic preganglionic neurons: implications for transneuronal labeling studies. Brain Res. 1993; 617:103–112. [PubMed: 8397044]

John J, Kumar VM. Effect of NMDA lesion of the medial preoptic neurons on sleep and other functions. Sleep. 1998; 21:587–598. [PubMed: 9779518]

Jones BE, Bobillier P, Pin C, Jouvet M. The effect of lesions of catecholamine-containing neurons upon monoamine content of the brain and EEG and behavioral waking in the cat. Brain Res. 1973; 58:157–177. [PubMed: 4581335]

Kaitin KI. Preoptic area unit activity during sleep and wakefulness in the cat. Exp Neurol. 1984; 83:347–357. [PubMed: 6692872]

Leak RK, Card JP, Moore RY. Suprachiasmatic pacemaker organization analyzed by viral transynaptic transport. Brain Res. 1999; 819:23–32. [PubMed: 10082857]

Lee RS, Steffensen SC, Henriksen SJ. Discharge profiles of ventral tegmental area GABA neurons during movement, anesthesia, and the sleep-wake cycle. J Neurosci. 2001; 21:1757–1766. [PubMed: 11222665]

Luo AH, Georges FE, Aston-Jones GS. Novel neurons in ventral tegmental area fire selectively during the active phase of the diurnal cycle. Eur J Neurosci. 2008; 27:408–422. [PubMed: 18215237]

Maeda H, Mogenson GJ. An electrophysiological study of inputs to neurons of the ventral tegmental area from the nucleus accumbens and medial preoptic-anterior hypothalamic areas. Brain Res. 1980; 197:365–377. [PubMed: 7407561]

Maloney KJ, Mainville L, Jones BE. c-Fos expression in dopaminergic and GABAergic neurons of the ventral mesencephalic tegmentum after paradoxical sleep deprivation and recovery. Eur J Neurosci. 2002; 15:774–778. [PubMed: 11886456]

McClung CA, Sidiropoulou K, Vitaterna M, Takahashi JS, White FJ, Cooper DC, Nestler EJ. Regulation of dopaminergic transmission and cocaine reward by the Clock gene. Proc Natl Acad Sci USA. 2005; 102:9377–9381. [PubMed: 15967985]

Moore, R. Entrainment pathways and the functional organization of the circadian system. In: Buijs, R.; Kalsbeek, A.; Romijn, H.; Pennartz, C.; Mirmiran, M., editors. Hypothalamic Integration of Circadian Rhythms. Elsevier; Amsterdam: 1996. p. 103-119.

Moore, R. Chemical neuroanatomy of the mammalian circadian system. In: Redfern, P.; Lemmer, B., editors. Physiology and Pharmacology of Biological Rhythms. Springer; New York: 1997. p. 79-93.

Moore RY, Eichler VB. Loss of a circadian adrenal corticosterone rhythm following suprachiasmatic lesions in the rat. Brain Res. 1972; 42:201–206. [PubMed: 5047187]

Morin LP, Shivers KY, Blanchard JH, Muscat L. Complex organization of mouse and rat suprachiasmatic nucleus. Neuroscience. 2006; 137:1285–1297. [PubMed: 16338081]

Mugnaini, E.; Oertel, W. An atlas of the distribution of GABAergic neurons and terminals in the rat CNS as revealed by GAD immunohistochemistry. In: Bjorklund, A.; Hokfelt, T., editors. Handbook of Chemical Neuroanatomy. Elsevier; Amsterdam: 1985. p. 436-608.

O'Donnell P, Lavin A, Enquist LW, Grace AA, Card JP. Interconnected parallel circuits between rat nucleus accumbens and thalamus revealed by retrograde transynaptic transport of pseudorabies virus. J Neurosci. 1997; 17:2143–2167. [PubMed: 9045740]

Phillipson OT. Afferent projections to the ventral tegmental area of Tsai and interfascicular nucleus: a horseradish peroxidase study in the rat. J Comp Neurol. 1979; 187:117–143. [PubMed: 489776]

Pickard GE, Smeraski CA, Tomlinson CC, Banfield BW, Kaufman J, Wilcox CL, Enquist LW, Sollars PJ. Intravitreal injection of the attenuated pseudorabies virus PRV Bartha results in infection of the hamster suprachiasmatic nucleus only by retrograde transsynaptic transport via autonomic circuits. J Neurosci. 2002; 22:2701–2710. [PubMed: 11923435]

Pompeiano M, Cirelli C, Tononi G. Immediate-early genes in spontaneous wakefulness and sleep: expression of c-fos and NGFI-A mRNA and protein. J Sleep Res. 1994; 3:80–96. [PubMed: 10607112]

Rinaman L, Card JP, Enquist LW. Spatiotemporal responses of astrocytes, ramified microglia, and brain macrophages to central neuronal infection with pseudorabies virus. J Neurosci. 1993; 13:685–702. [PubMed: 8381171]

Risold PY, Swanson LW. Chemoarchitecture of the rat lateral septal nucleus. Brain Res Brain Res Rev. 1997a; 24:91–113. [PubMed: 9385453]

Risold PY, Swanson LW. Connections of the rat lateral septal complex. Brain Res Brain Res Rev. 1997b; 24:115–195. [PubMed: 9385454]

Roberts DC, Brebner K, Vincler M, Lynch WJ. Patterns of cocaine self-administration in rats produced by various access conditions under a discrete trials procedure. Drug Alcohol Depend. 2002; 67:291–299. [PubMed: 12127200]

Satinoff E, Valentino D, Teitelbaum P. Thermoregulatory cold-defense deficits in rats with preoptic/anterior hypothalamic lesions. Brain Res Bull. 1976; 1:553–565. [PubMed: 1021211]

Schultz W. Behavioral theories and the neurophysiology of reward. Annu Rev Psychol. 2006; 57:87–115. [PubMed: 16318590]

Simerly RB, Swanson LW. Projections of the medial preoptic nucleus: a *Phaseolus vulgaris* leucoagglutinin anterograde tract-tracing study in the rat. J Comp Neurol. 1988; 270:209–242. [PubMed: 3259955]

Simerly RB, Gorski RA, Swanson LW. Neurotransmitter specificity of cells and fibers in the medial preoptic nucleus: an immunohistochemical study in the rat. J Comp Neurol. 1986; 246:343–363. [PubMed: 2422228]

Smeraski CA, Sollars PJ, Ogilvie MD, Enquist LW, Pickard GE. Suprachiasmatic nucleus input to autonomic circuits identified by retrograde transsynaptic transport of pseudorabies virus from the eye. J Comp Neurol. 2004; 471:298–313. [PubMed: 14991563]

Stefanick ML. The circadian patterns of spontaneous seminal emission, sexual activity and penile reflexes in the rat. Physiol Behav. 1983; 31:737–743. [PubMed: 6665062]

Steffensen SC, Svingos AL, Pickel VM, Henriksen SJ. Electrophysiological characterization of GABAergic neurons in the ventral tegmental area. J Neurosci. 1998; 18:8003–8015. [PubMed: 9742167]

Stephan FK, Zucker I. Circadian rhythms in drinking behavior and locomotor activity of rats are eliminated by hypothalamic lesions. Proc Natl Acad Sci USA. 1972; 69:1583–1586. [PubMed: 4556464]

Swanson, L. Brain Maps III: Structure of the rat Brain. Academic; Oxford: 2003.

Swanson LW, Cowan WM. The efferent connections of the suprachiasmatic nucleus of the hypothalamus. J Comp Neurol. 1975; 160:1–12. [PubMed: 803516]

Terman M, Terman JS. Circadian rhythm of brain self-stimulation behavior. Science. 1970; 168:1242–1244. [PubMed: 5442714]

Van Bockstaele EJ, Pickel VM. GABA-containing neurons in the ventral tegmental area project to the nucleus accumbens in rat brain. Brain Res. 1995; 682:215–221. [PubMed: 7552315]

Vrang N, Larsen PJ, Moller M, Mikkelsen JD. Topographical organization of the rat suprachiasmatic-paraventricular projection. J Comp Neurol. 1995; 353:585–603. [PubMed: 7759617]

Watts AG, Swanson LW. Efferent projections of the suprachiasmatic nucleus: II. Studies using retrograde transport of fluorescent dyes and simultaneous peptide immunohistochemistry in the rat. J Comp Neurol. 1987; 258:230–252. [PubMed: 2438309]

Watts AG, Swanson LW, Sanchez-Watts G. Efferent projections of the suprachiasmatic nucleus: I. Studies using anterograde transport of *Phaseolus vulgaris* leucoagglutinin in the rat. J Comp Neurol. 1987; 258:204–229. [PubMed: 3294923]

White FJ, Wang RY. Comparison of the effects of chronic haloperidol treatment on A9 and A10 dopamine neurons in the rat. Life Sci. 1983; 32:983–993. [PubMed: 6827927]

Wise RA. Dopamine, learning and motivation. Nat Rev Neurosci. 2004; 5:483–494. [PubMed: 15152198]

Yamaguchi T, Sheen W, Morales M. Glutamatergic neurons are present in the rat ventral tegmental area. Eur J Neurosci. 2007; 25:106–118. [PubMed: 17241272]

Yan L, Takekida S, Shigeyoshi Y, Okamura H. Per1 and Per2 gene expression in the rat suprachiasmatic nucleus: circadian profile and the compartment-specific response to light. Neuroscience. 1999; 94:141–150. [PubMed: 10613504]

Yim CY, Mogenson GJ. Electrophysiological studies of neurons in the ventral tegmental area of Tsai. Brain Res. 1980; 181:301–313. [PubMed: 7350968]

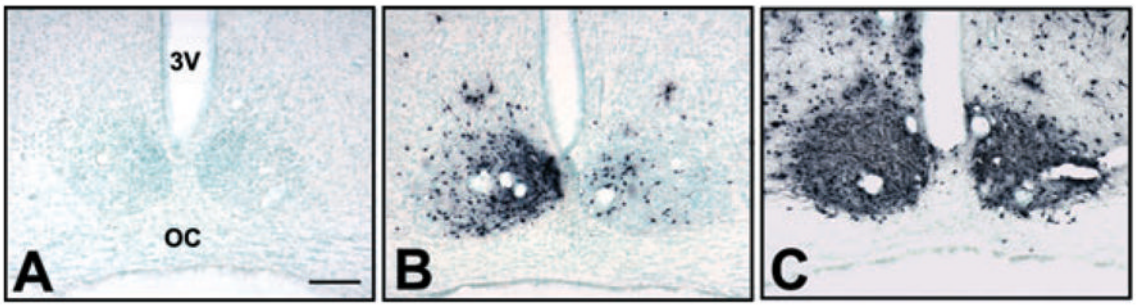

Fig. 1.

Photomicrographs of frontal sections through SCN stained for PRV at different time points following injection into VTA. The left side of all images is ipsilateral to the PRV/CTb injection site in VTA. (A) No labeling was present in SCN at 36 h post-injection when labeling in direct SCN afferents was present (see Figs 3, 4 and 5A and D). (B) By 48 h, labeling was consistently observed in the ipsilateral and, to a lesser extent, in the contralateral SCN. (C) By 60 h, labeling was substantial in both the ipsilateral and contralateral SCN. Midline is center and dorsal is up for all images. 3 V, third ventricle; OC, optic chiasm. Scale bar, 200 μm.

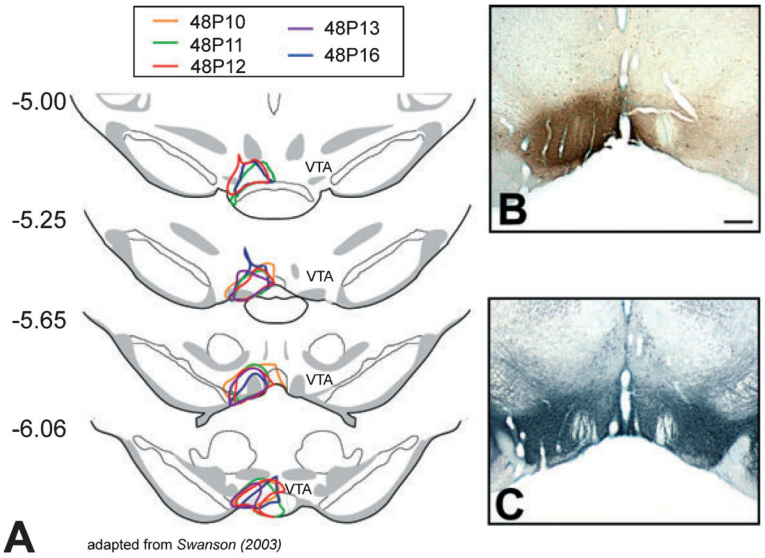

Fig. 2.

Drawings and photomicrographs of frontal sections through VTA showing PRV/CTb injection sites. Because PRV is avidly transported away from the site of injection, CTb and TH immunoreactivity were used to localize the injection. (A) Schematic outlines of injection sites as defined by CTb immunoreactivity at rostral–caudal levels of VTA from all five 48-h survival time-point animals. Numbers at left indicate distance (mm) posterior to bregma. (B) Frontal photomicrograph of CTb immunoreactivity at the largest extent of the injection site (~−5.65 mm from bregma) for Case 48P10. (C) Adjacent section of Case 48P10 stained for TH and used to define the boundaries of VTA. Midline is center and dorsal is up for all images. Scale bar, 500 μm (B and C).

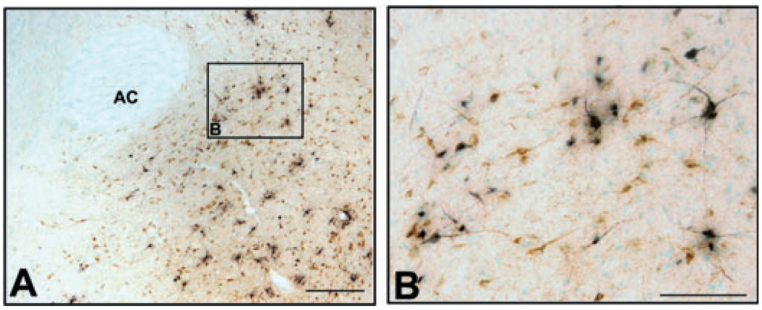

Fig. 3.

Photomicrographs of frontal sections through NAC showing PRV (black)- and CTb (brown)-labeled neurons at 36 h following injection of PRV/CTb cocktail into VTA. (A) Low-magnification photomicrograph of NAC. (B) High-magnification photo of inset shown in (A). Midline is at the right edge of the image and dorsal is up. AC, anterior commissure. Scale bars, 250 μm (A), 100 μm (B).

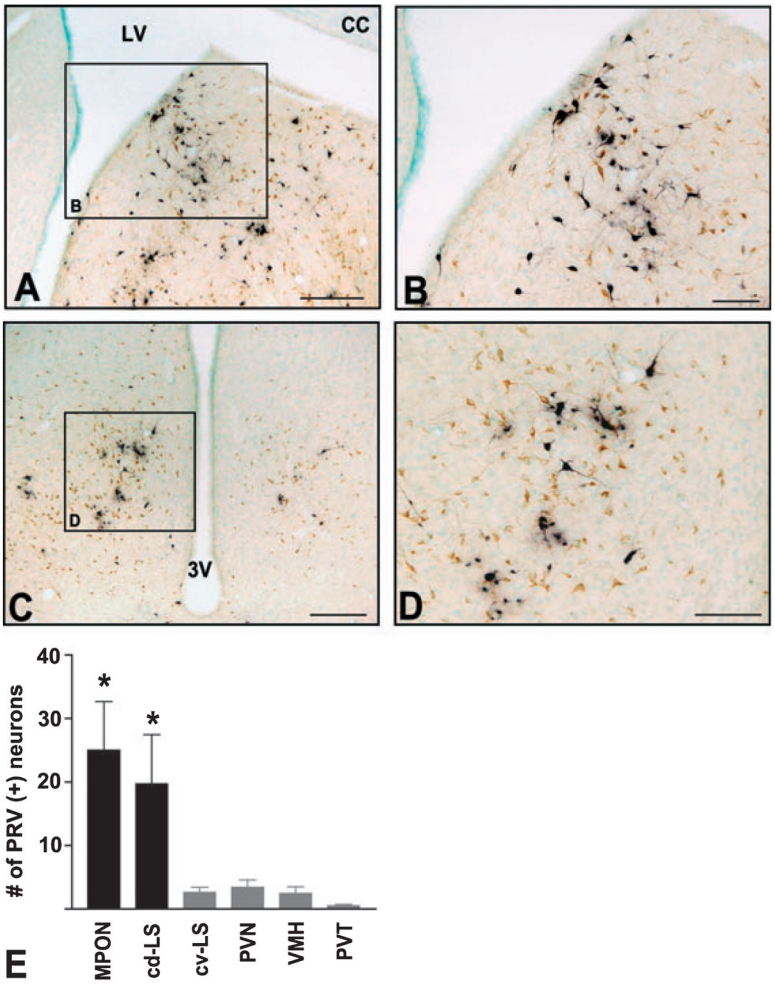

Fig. 4.

Photomicrographs and quantification of frontal sections showing PRV (black) and CTb (brown) immunoreactivity in putative relay nuclei at 36 h following injection into VTA. (A and C) Low-magnification photomicrographs of frontal sections showing (A) cd-LS and (C) MPON. (B and D) High-magnification photomicrographs of insets in A and C, respectively. Midline is at the right edge of the image in A and center in C. Dorsal is up in all panels. LV, lateral ventricle; CC, corpus callosum; 3 V, third ventricle. (E) Quantification of PRV+ neurons in ipsilateral cd-LS, MPON and nearby nuclei at 36 h following injection into VTA (cv-LS, caudal-ventral lateral septum; PVN, paraventricular nucleus of the hypothalamus; VMH, ventromedial hypothalamus; PVT, paraventricular nucleus of the thalamus). The *y*-axis indicates the average number of PRV+ neurons per section in the hemisphere ipsilateral to the PRV/CTb injection in VTA. Labeling was higher in cd-LS and MPON than in the four other areas (*$P < 0.05$ vs. areas in grey bars). Scale bars, 250 μm (A and C), 100 μm (B and D).

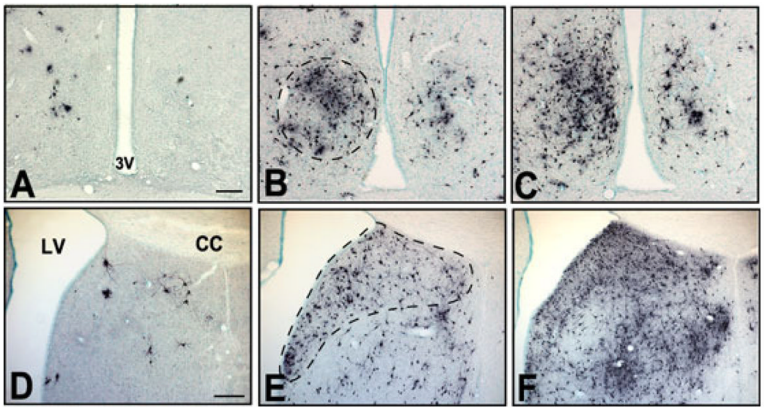

Fig. 5.

Photomicrographs of frontal sections showing PRV labeling in (A–C) medial preoptic area and (D–F) lateral septum at (A and D) 36 h, (B and E) 48 h and (C and F) 60 h following PRV/CTb injection into VTA. Broken lines in B and E indicate areas of heavy labeling corresponding to the subregions MPON and cd-LS, respectively. These subregions were targets of subsequent lesion studies (Figs 6 and 7). The left side of all panels is ipsilateral to the injection site. Midline is center in A–C and at the right edge of the image in panels D–F. 3 V, third ventricle; LV, lateral ventricle. Scale bars, 200 μm (in A for A–C and in D for D–F).

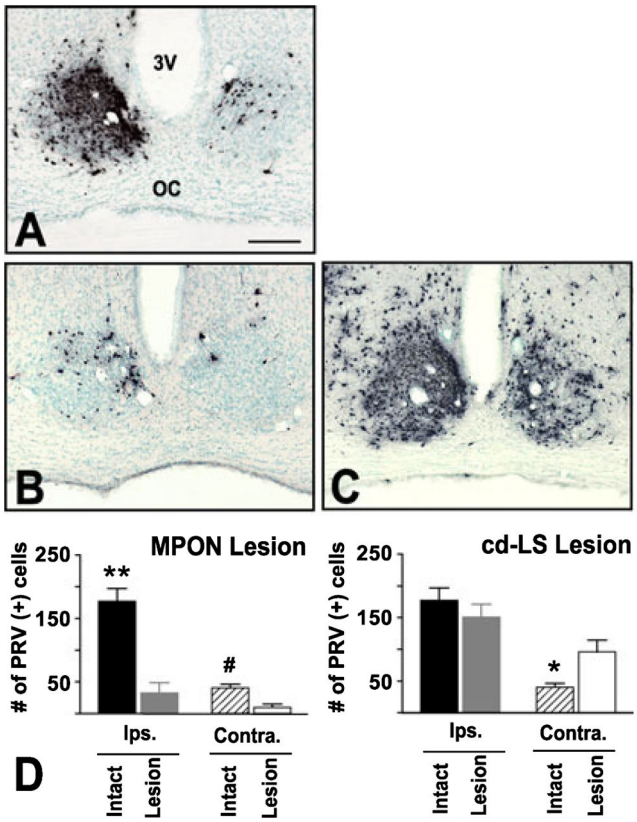

Fig. 6.

(A–C) Photomicrographs and quantification of frontal sections showing PRV labeling in SCN 48 h after a PRV/CTb injection into VTA from (A) intact, (B) MPON- or (C) cd-LS-lesioned animals. The left side of all panels is ipsilateral to the injection site. 3 V, third ventricle; OC, optic chiasm. (D and E) Average number of neurons labeled in SCN with PRV in (D) MPON-and (E) cd-LS-lesioned animals. (B and D) Lesion of MPON reduced PRV labeling in both ipsilateral ($^{**}P < 0.001$) and contralateral ($^{\#}P < 0.01$) SCN. (C and E) Lesion of the cd-LS did not change PRV labeling in ipsilateral SCN, but increased labeling in contralateral SCN ($^{*}P < 0.05$). Scale bar, 200 μm.

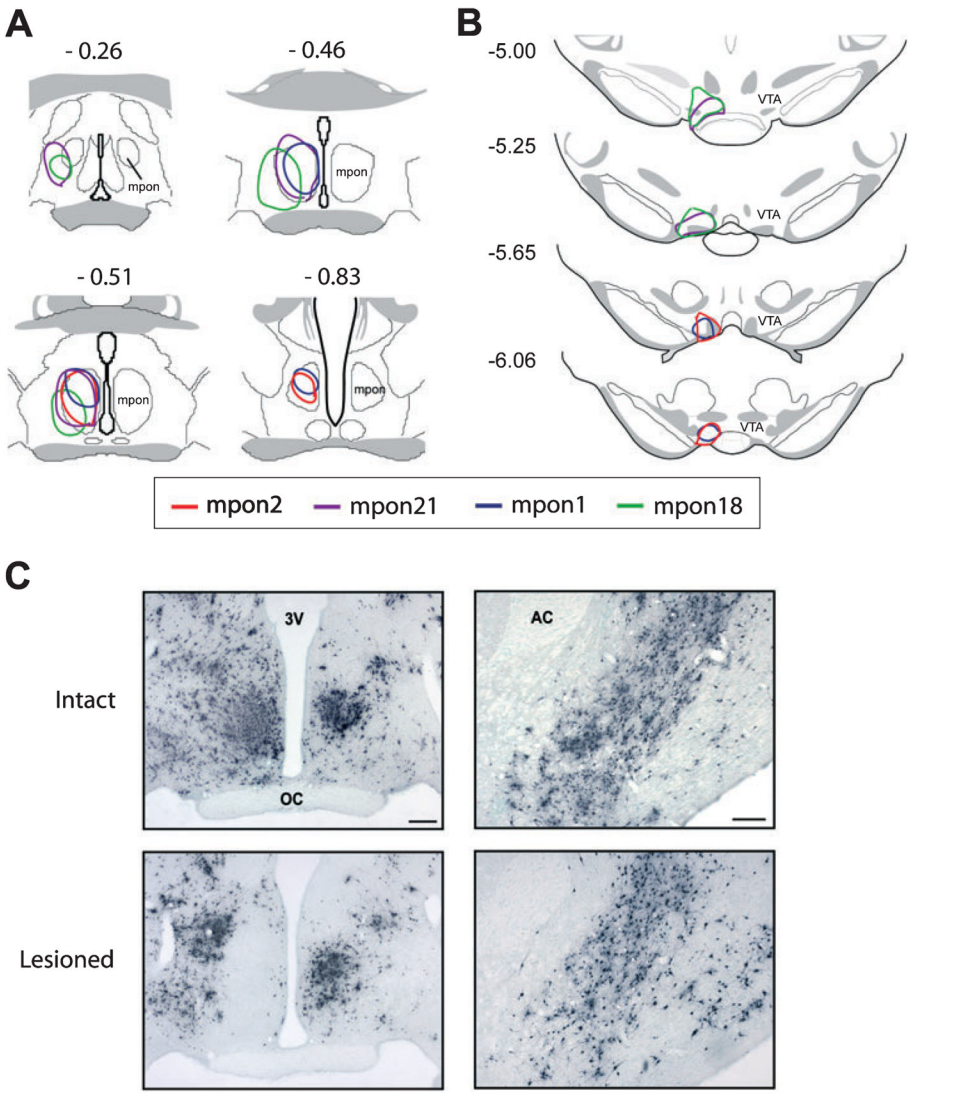

Fig. 7.

(A and B) Drawings of frontal sections through MPON and VTA showing lesion and PRV/CTb injection sites. (A) Schematic outlines of ibotenic acid lesion sites in MPON as defined by PRV immunoreactivity from four animals. Numbers above each drawing indicate distance (mm) posterior to bregma. (B) Schematic outlines of PRV/CTb injection sites in VTA as defined by CTb immunoreactivity from the same four animals described in A. Numbers at left indicate distance (mm) posterior to bregma. (C, left) Photomicrographs of frontal sections of PRV labeling in intact and MPON-lesioned animals 48 h following PRV/CTb injection into VTA. (C, right) PRV labeling of nucleus accumbens 48 h post-VTA injection in intact and MPON-lesioned animals. Lesion of the MPON did not significantly change PRV labeling in the nucleus accumbens, another direct VTA afferent. Midline is center in C, left, and the right edge of image in C, right. 3 V, third ventricle; OC, optic chiasm; AC, anterior commissure. Scale bars, 200 μm.

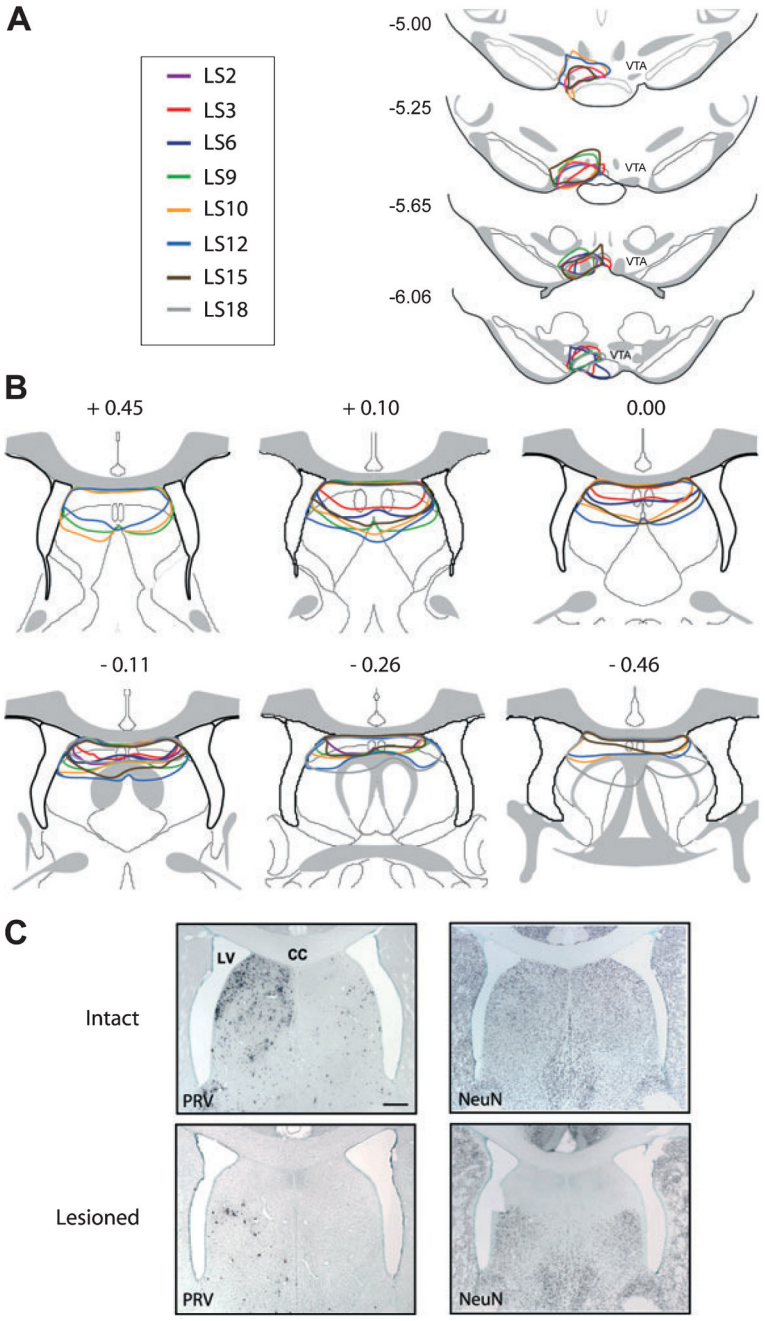

Fig. 8.

(A and B) Drawings of frontal sections through cd-LS and VTA showing PRV/CTb and lesion injection sites, respectively. (A) Schematic outlines of PRV/CTb injection sites in VTA as defined by CTb immunoreactivity from eight animals. Numbers at left indicate distance (mm) posterior to bregma. (B) Schematic outlines of ibotenic acid lesion sites in cd-LS as defined by NeuN immunoreactivity from the same eight animals described in A. Numbers above each drawing indicate distance (mm) relative to bregma. (C, left) Photomicrographs of frontal sections of PRV labeling in intact and cd-LS-lesioned animals 48 h following PRV/CTb injection into VTA. (C, right) NeuN immunoreactivity from sections adjacent to C, left. Because PRV labeling is largely confined to the ipsilateral cd-LS

in intact animals (C, upper left), NeuN immunoreactivity was used define lesioned areas in both ipsilateral and contralateral hemispheres. LV, lateral ventricle; CC, corpus callosum. Scale bar, 200 μm (C).

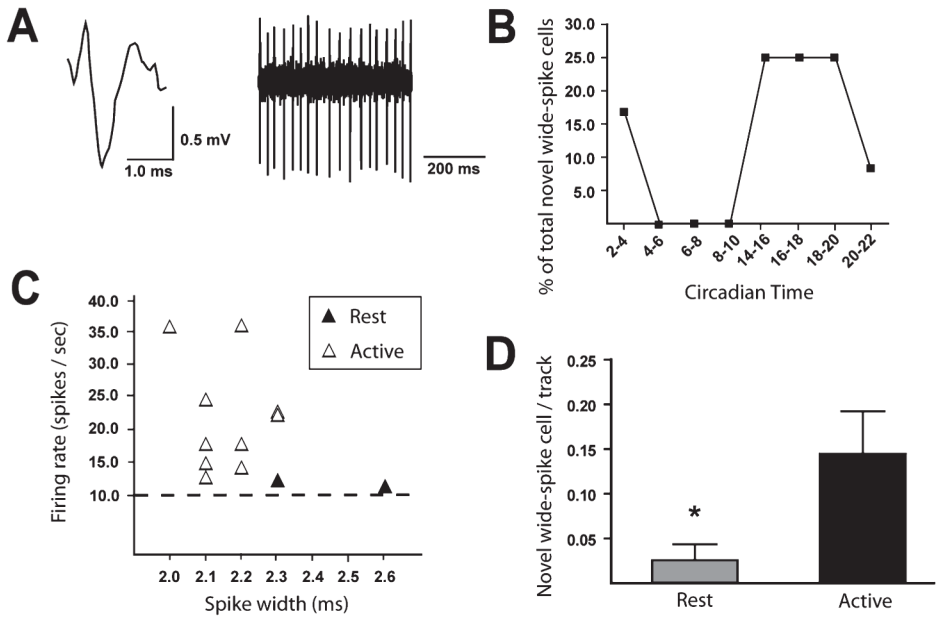

Fig. 9.

VTA novel wide-spike neurons exhibited a circadian rhythm in impulse activity. These neurons were characterized by their wide waveforms and tonically fast-firing impulse activity. (A) Digitized waveform (upper left), spike train (upper right). (B) Novel wide-spike neuron proportions through the circadian cycle. Each point represents the proportion of total novel wide-spike neurons found during that respective CT range. (C) Novel wide-spike neurons in active and resting phases are plotted as a function of their firing rate and spike widths. Horizontal dotted line indicates 10 spikes/s, the minimum firing rate of a neuron categorized as a novel wide-spike. More novel wide-spike neurons were recorded during the active phase than in the resting phase ($P < 0.05$). (D) The number of spontaneously active novel wide-spike neurons per electrode track as recorded during each circadian phase. Bars are SEM; $*P = 0.02$. Novel wide-spike neurons selectively fired during the active circadian phase.